Bioconjugate Chemistry

Article

pubs.acs.org/bc

Self-Immobilization of Car9 Fusion Proteins within High Surface Area Silica Sol–Gels and Dynamic Control of Protein Release

Wenlan Yang, Brittney Hellner, and François Baneyx*

Department of Chemical Engineering, Box 351750, University of Washington, Seattle, Washington 98195, United States

Supporting Information

ABSTRACT: Protein entrapment within silica matrices during sol–gel formation is an effective way of producing biocatalysts with high load, activity retention, and minimal leaching. On the other hand, mesoporous silica materials have been favored for diffusional control of protein delivery because of their regular pore size and morphology and in spite of the drawback of requiring post-synthesis loading with cargo proteins. Here, we describe a hybrid technology in which fusion of the silica-binding Car9 dodecapeptide to model fluorescent proteins allows for their simultaneous entrapment and surface immobilization within sol–gel monoliths that can be fabricated in air and oil phases. Spherical particles produced by injecting a mixture of silicic acid and Car9-tagged proteins in silicone oil exhibit high surface area (>400 m^2/g), 15-nm-diameter mean pore size and homogeneous protein loading. Incubation in arginine-containing buffer disrupts the interaction between Car9 extensions and silica surfaces and triggers the continuous or discontinuous (on/off) release of cargo proteins with pH-tunable kinetics. This simple approach for producing hybrid silica materials that stably encapsulate and release one or more Car9-tagged proteins in a single step may prove useful for applications requiring dynamic control of protein concentration.

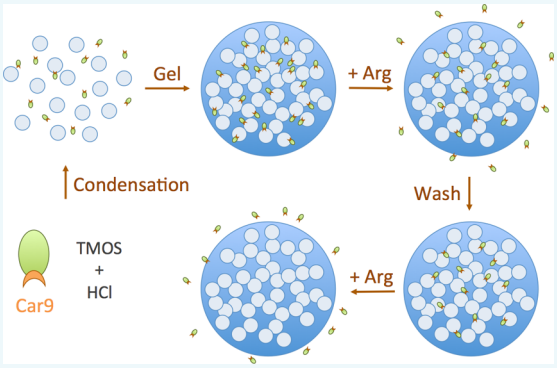

INTRODUCTION

Entrapment of proteins within porous three-dimensional matrices allows for their controlled delivery and long-term storage and operation, and enables a broad range of applications in biomedicine, diagnostics, biosensing, biocatalysis, and bioremediation. Among the inorganic materials studied thus far, silica sol–gels have proven particularly valuable due to their ease of preparation under ambient conditions, optical transparency, mechanical stability, negligible swelling, and biocompatibility (for recent reviews, see refs 1–4). Silica sol–gels are most commonly prepared by hydrolysis of silicon alkoxide precursors under acidic or basic conditions followed by polycondensation of the hydroxylated units into oligomers and colloidal particles that eventually associate to form a continuous, percolated network terminated by surface silanol groups.[5−7] Proteins can be encapsulated in a functional state during the growth of such networks if added in buffered solutions to prehydrolyzed alkoxides[8] or to appropriately processed solutions of sodium silicate if the polypeptide of interest is sensitive to the alcohols that are released during polycondensation.[9] Sol–gel pore size and porosity can be coarsely adjusted by manipulating the pH (gelation under acidic conditions favors the growth of short linear chains over extended tridimensional polymers and thus decreases pore size), by supplying the reaction with additives, or by modifying the processing conditions.[6,10,11] A much finer degree of control over the dimension, structure, and morphology of the pores can be achieved by performing the sol–gel reaction in the presence of self-assembled organic templates (e.g., surfactants and polymers) which are removed upon completion of synthesis.[12−16] While these mesoporous silica nanoparticle (MSN) materials have high surface areas and large accessible pore volumes, the conditions used for their synthesis are generally harsh.[17] This means that proteins must be loaded into preformed MSN networks of optimized morphology and chemistry by an impregnation step.

At present, traditional sol–gel processing in the presence of proteins is chiefly employed for the production of biosensors and biocatalysts. For these applications, pores should be large enough to permit the diffusion of reactants and products, but small enough to prevent entrapped enzymes from leaching into the surrounding fluid (i.e., ∼5–10 nm for most enzymes).[18] By contrast, controlled protein release schemes have mainly focused on MSNs because the diffusion kinetics of entrapped species can be controlled by tuning pore size and morphology; by forming cleavable covalent bonds (e.g., disulfides) between a genetically modified guest protein and a chemically modified pore surface; or by making use of more esoteric gating mechanisms such as nanovalves.[3,17,19]

Diatoms, sponges, and higher plants mineralize nanopatterned amorphous silica as skeletal material under genetic control and under physiological conditions.[20,21] In the diatom

Received: July 20, 2016
Revised: August 27, 2016
Published: September 3, 2016

DOI: 10.1021/acs.bioconjchem.6b00406
Bioconjugate Chem. 2016, 27, 2450–2459

Cylindrotheca fusiformis, the process is mediated in part by long chain polyamines and by silaffin peptides such as R5 (SSKKSGSYSGSKGSKRRIL), a repeating unit of the silaffin precursor protein that undergoes extensive post-translational modifications.[22,23] In its unmodified, synthetic form, R5 remains capable of catalyzing the precipitation of ∼500 nm spherical silica particles when added at high concentrations to phosphate-buffered solutions of silicic acid.[22,24] The process is complete on the order of seconds and is thought to involve: self-association of peptides into supramolecular structures via salt bridge formation between the guanidine groups of arginine residues in the RRIL motif and phosphate anions; acid−base catalysis of siloxane bond formation between silicic acid monomers and/or colloidal silica particles mediated by the amino groups of critical lysine residues;[25] and finally, polycondensation into particles that grow to encapsulate the templating peptide assemblies.[26,27]

The biosilicification activity of R5 has been exploited to coprecipitate functional enzymes and nanoparticles within silica matrices.[28,29] Unfortunately, the approach requires large amounts of synthetic R5 (∼10 mg/mL) in addition to a purified target protein and may not be effective for the coprecipitation of small bioactive polypeptides.[30] To circumvent these issues, R5 and other silaffin-derived peptides have been genetically fused to the N- and C-termini of green fluorescent protein (GFP), glucose oxidase, phosphodiesterase, and organophosphate hydrolase.[31−33] Such fusion proteins support their autoentrapment by triggering silica precipitation from silicic acid solutions in about 5 min and at concentrations that are 14- to 17-times lower those used for R5 peptide-mediated encapsulation.[33] While they are suitable for biocatalysis and biosensing, these composite materials have low surface area,[34] and because they permanently encase guest proteins, they are not suitable for applications requiring diffusional or stimuli-controlled protein release.

Our now routine ability to isolate solid-binding peptides that bind to virtually any material through display technologies provides a powerful alternative to the use of natural biomineralizing proteins for materials synthesis, molecular biomimetics, and bionanotechnology.[35−41] Previously, we identified the dodecapeptide Car9 (DSARGFKKPGKR) for its ability to bind to the edges of graphitic materials[42] and later discovered that it also exhibits high affinity for silica.[43] The interaction survives in the presence of high salt concentrations but can be competitively disrupted by addition of free lysine or arginine,[43] which allows rapid and inexpensive affinity purification of Car9 fusion proteins on silica beads, and their oriented immobilization and reversible microcontact printing onto glass substrates.[43,44]

In this study, we demonstrate that fusion of the Car9 extension to model fluorescent proteins accelerates the rate of silicic acid polycondensation in Tris buffer without causing silica precipitation. As a result, Car9-tagged proteins become homogeneously entrapped within, and simultaneously non-covalently immobilized onto, high surface area sol−gel networks that can be manufactured in air and oil phases. Incubation in arginine-containing buffer triggers the release of cargo proteins in a continuous or discontinuous manner and with kinetics that can be adjusted by manipulating particle shape and size, protein load, and solution pH.

RESULTS AND DISCUSSION

Car9 is Less Effective than R5 at Catalyzing Silica Precipitation in Phosphate-Containing Buffer. To determine if Car9 fusion proteins would induce silica precipitation from silicic acid precursors like R5 fusions do,[31−33] we made use of sfGFP-Car9, a variant of superfolder green fluorescent protein (sfGFP)[45] bearing a C-terminal Car9 tag.[43] Previously, Nam et al. showed that a structurally similar GFP-R5 fusion protein catalyzed biosilicification within 5 min when added at a concentration of 0.7 mg/mL (21.5 μM) to a 100 mM solution of prehydrolyzed tetramethoxysilane (TMOS; Figure 1A).[33] When sfGFP-Car9 was used at the same concentration and under the same experimental conditions, we observed no silica precipitation or gelation after up to 1 h incubation at room temperature. However, centrifugation of samples that had been incubated at 23 °C for

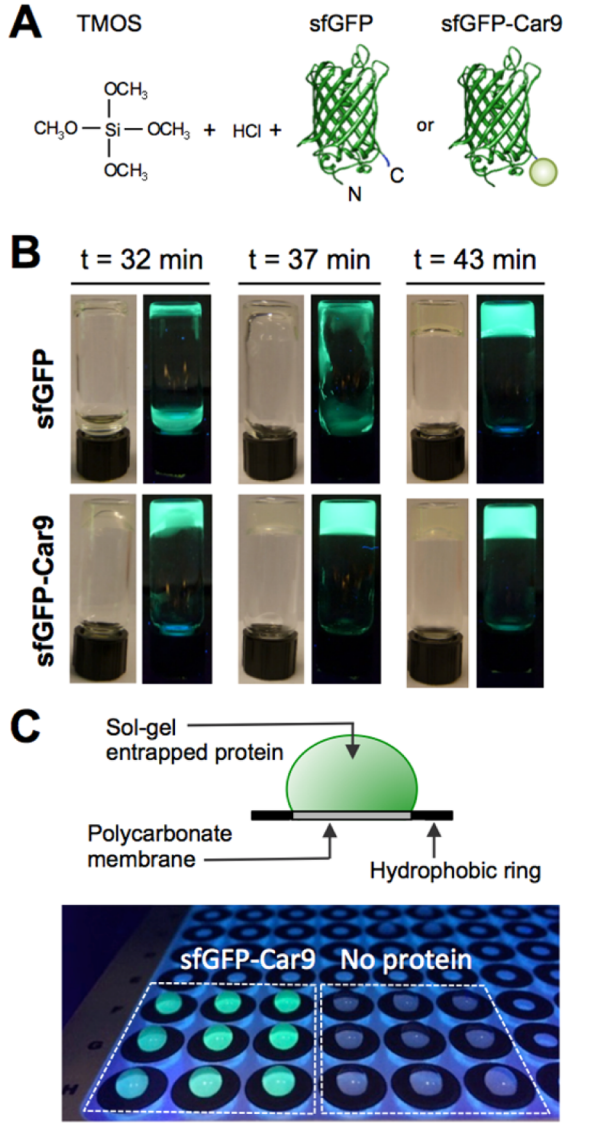

Figure 1. Entrapment of sfGFP and sfGFP-Car9 within silica sol−gels. (A) Schematic illustration of the process and proteins. (B) Ability of sfGFP and sfGFP-Car9 (10 μM) to drive sol−gel formation was compared by inversion experiments at the indicated time points. Vials were photographed under ambient and UV light. (C) Formation of hemispheroidal sol−gel particles on ChemoTx plates.

DOI: 10.1021/acs.bioconjchem.6b00406
Bioconjugate Chem. 2016, 27, 2450−2459

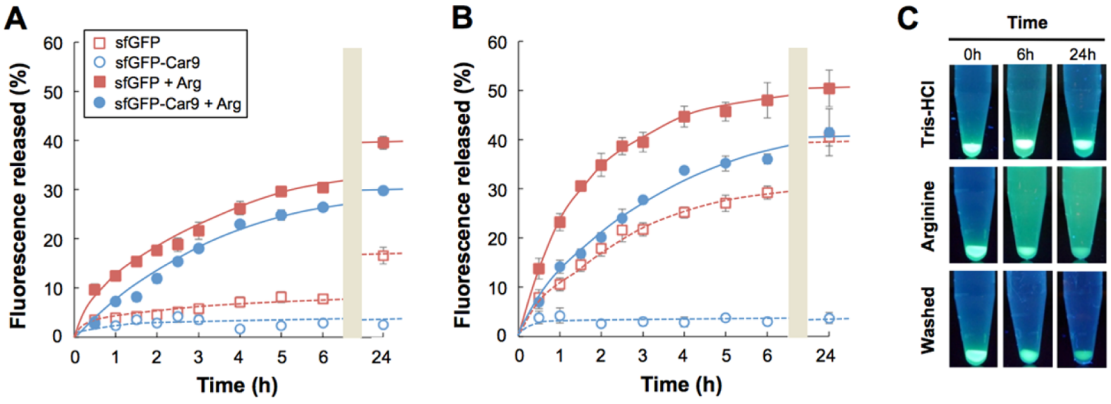

Figure 2. Effect of pH and arginine on the release of sfGFP and sfGFP-Car9 from hemispheroidal sol–gel particles. sfGFP or sfGFP-Car9 (10 μM) entrapped in hemispheroidal silica particles were incubated at room temperature with shaking in 1 mL of 20 mM Tris-HCl buffered at pH 7.5 (A) or 8.5 (B) and containing or lacking 1 M arginine (Arg). The fluorescence released in the supernatants was assayed at the indicated time points. Error bars correspond to triplicate independent experiments. A value of 100% corresponds to the fluorescence of a 10 μM solution of sfGFP or sfGFP-Car9. (C) Appearance of particles and supernatants under UV illumination at 365 nm following 0, 6, and 24 h incubation in Tris-HCl or arginine-containing solutions. The lower panel shows the appearance of arginine-treated particles following removal of the supernatant and buffer wash.

24 h led to complete depletion of the supernatant fluorescence and the appearance of a highly fluorescent pellet. We conclude that Car9 is much less effective than R5 at endowing GFP with silica-precipitating activity in spite of the fact that the two extensions have similar pI (11.1 for Car9 vs 11.1 for R5) and specify a comparable number of basic residues (3 lysines and 2 arginines for Car9 vs 4 lysines and 2 arginines for R5). The difference may be related to the structural and chemical context in which the lysine residues of the common KXXK motif (where X is any amino acid) are presented to the solvent[46] and to the absence of an RRIL motif which has been proposed to help template silica precipitation by clustering R5 segments through electrostatic interactions between the guanidine groups of arginine residues and divalent phosphate ions.[27]

Entrapment of Car9-Tagged Proteins in Hemispheroidal Silica Sol–Gels. Because it lacks the strong silica-precipitating activity of R5 but exhibits chemically addressable silica-binding activity,[43,44] we hypothesized that the Car9 extension might prove useful to homogeneously and reversibly tether proteins within sol–gel networks. We determined that incubation of a 1 M solution of prehydrolyzed TMOS with a Tris-buffered solution under mildly acidic conditions to reduce the rate of silicic acid polycondensation led to sol–gel formation in a little over 1 h (t = 71.3 ± 6 min). Addition of 10 μM (~0.3 mg/mL) of sfGFP-Car9 to the mixture led to the formation of fluorescent monoliths in half that time (t = 35.3 ± 2.9 min). Interestingly, wild-type sfGFP, a 238 residues protein containing 20 lysines and 8 arginines, also accelerated the gelation process (t = 46 ± 3.6 min; Figure 1B). Yet, the increase in the rate of sol–gel formation observed with sfGFP-Car9 could be entirely attributed to the Car9 extension as there was no significant difference in gelation times between sfGFP and sfGFP-CT43, a fusion protein between sfGFP and the CT43 zinc sulfide-binding dodecamer[47] (Figure S1 in Supporting Information).

To more conveniently handle protein-laden sol–gels, we developed a process to fabricate hemispheroidal monoliths by depositing 30 μL of protein–silicic acid solution onto circular polycarbonate membranes bounded by hydrophobic rings (Figure 1C). After 4 h incubation in sealed chambers to ensure complete polymerization, the particles were washed and transferred to Tris-HCl buffer for characterization of protein release kinetics.

Chemical Control of Car9-Tagged Protein Release. The equilibrium dissociation constant (K_d) between Car9-tagged proteins and silica surfaces is ~1 μM.[43] Although this interaction is not affected by high salt concentrations (up to 5 M NaCl or $MgCl_2$), it is competitively disrupted in the presence of 1 M arginine.[43,44] (Lysine solutions can be used for the same purpose but we did not use this amino acid because it fluoresces in the GFP excitation window.) To study the influence of Car9 tagging on protein release from sol–gels, we placed single hemispheroidal silica particles fabricated in the presence of sfGFP or sfGFP-Car9 in Tris-HCl solutions buffered at pH 7.5 or 8.5 and quantified the amount of fluorescence released in the supernatant as described in the Experimental Section.

In the absence of additive and at pH 7.5, about 7% of the encapsulated sfGFP leached out of the particles over a period of 6 h (assuming 100% entrapment and no protein denaturation during sol–gel formation). Protein leakage rose to 17% after 24 h and tapered off to 22% after 48 h (Figure 2A, open squares Table S1). Under the same conditions, no sfGFP-Car9 reached the supernatant indicating that the Car9 extension firmly anchors sfGFP to silica (Figure 2A, open circles). Inclusion of 1 M arginine triggered sfGFP-Car9 release: about 25% of the fusion protein was released over 6 h and there was little change in this number after overnight incubation. Supplementation of the buffer with arginine also increased the rate and extent of sfGFP leakage, presumably because high concentrations of this amino acid passivates the silica surface by forming ion pairs with negatively charged silanols (Figure 2A, closed symbols).

Raising the pH from 7.5 to 8.5, which increases the number of deprotonated surface silanols from 18% to 50% (the maximum degree of silica ionization),[48] magnified differences between the two proteins (Figure 2B,C). Whereas no sfGFP-Car9 was released from particles incubated in arginine-free buffer, sfGFP leaked into the solvent with 10-fold higher initial rates than at pH 7.5 (Figure 2B,C, open squares, Figure S2, Table S1). Incubation with arginine further increased sfGFP leaching and triggered the release of sfGFP-Car9 (Figure 2B). After 24 h, 42% of the entrapped sfGFP-Car9 and 50% of the encapsulated sfGFP had reached the supernatant. There was no

DOI: 10.1021/acs.bioconjchem.6b00406
Bioconjugate Chem. 2016, 27, 2450–2459

further release of either protein when incubation was pursued for an additional 24 h. However, the particles remained fluorescent (Figure 2C), indicating that about half of the protein load remains confined within the core of hemispheroidal sol–gel particles (Figure S3) or is released with kinetics that are too slow to be captured by our experiments. Why the arginine-mediated release of sfGFP-Car9 occurs with initial kinetics that are 50% slower than those of sfGFP is unclear, but it could be due to Car9-mediated cycles of binding and release and/or to subtle differences in pore structure associated with a different silicic acid condensation rate (Figure 1B).

To summarize, the Car9 tag catalyzes silica sol–gel formation and confines proteins to which it is fused to the inorganic matrix. Protein release is entirely dependent on the presence of a Car9-specific eluent such as arginine and the kinetics and extent of release can be tuned by manipulating the solution pH to modulate the biotic–abiotic interaction.

Entrapment of Car9-Tagged Proteins within Spherical Silica Sol–Gels. To better characterize the kinetics of arginine-induced protein release and avoid pore distortion effects caused by the action of capillary forces at the air/sol–gel interface (Figure S3), we developed a process in which a mixture of silicic acid and sfGFP-Car9 is injected into silicone oil to yield protein-loaded spherical particles of tunable sizes (Figure 3A). SEM imaging showed that the sol–gels thus produced consist of a connected network of fused silica spheres in the 50–100 nm range (Figure 3B). While nanosphere packing was generally tight, larger voids were not uncommon (Figure 3B, inset). Consistent with this morphological characterization, Barrett–Joyner–Halenda (BJH) analysis revealed that although there is a clear peak corresponding to a mean pore radius of ~7.5 nm, a broad distribution of larger pores is also present (Figure 3C). The surface area of particles subjected to critical point drying was ~410 m^2/g, about 2- to 3-fold less than that of the best MSN materials. However, it was comparable to that of other sol–gels produced by chemical conversion of silicon alkoxides,[49−51] and over 55-fold higher than the surface area reported for bioprecipitated silica.[34] Overall, the pore size and large surface area of the spherical silica sol–gels particles produced in silicone oil are well suited for protein entrapment.

Arginine-Triggered Release of sfGFP-Car9 from Spherical Sol–Gels. Preliminary experiments revealed that when particles produced in silicone oil were washed in buffer and incubated with arginine to liberate entrapped sfGFP-Car9, the supernatant fluorescence stopped rising after 1 h, started to decrease after 3 h, and reached background levels after 24 h incubation (Figure S4). This behavior is indicative of a sfGFP-Car9 unfolding event mediated by exposure to silicone oil.[52] It was corrected by including the detergent Tween 20 in the wash buffer to remove surface-adsorbed oil and eliminate interfacial protein denaturation (Figure S4). With the exception of Figure S6, all subsequent protein release experiments were conducted in solutions buffered at pH 8.5 to magnify differences between protein release profiles.

Figure 4 shows that unlike with hemispheroidal particles solidified in air, a small amount of sfGFP-Car9 escaped the spherical particles during incubation in pH 8.5 buffer alone (10% or 11% of the original protein load was released after 24 h, and 16% or 21% after 48 h for 1- or 2-mm-radius particles, respectively). The reasons for this discrepancy are unclear but may be related to constriction of the pore mouths in the outer

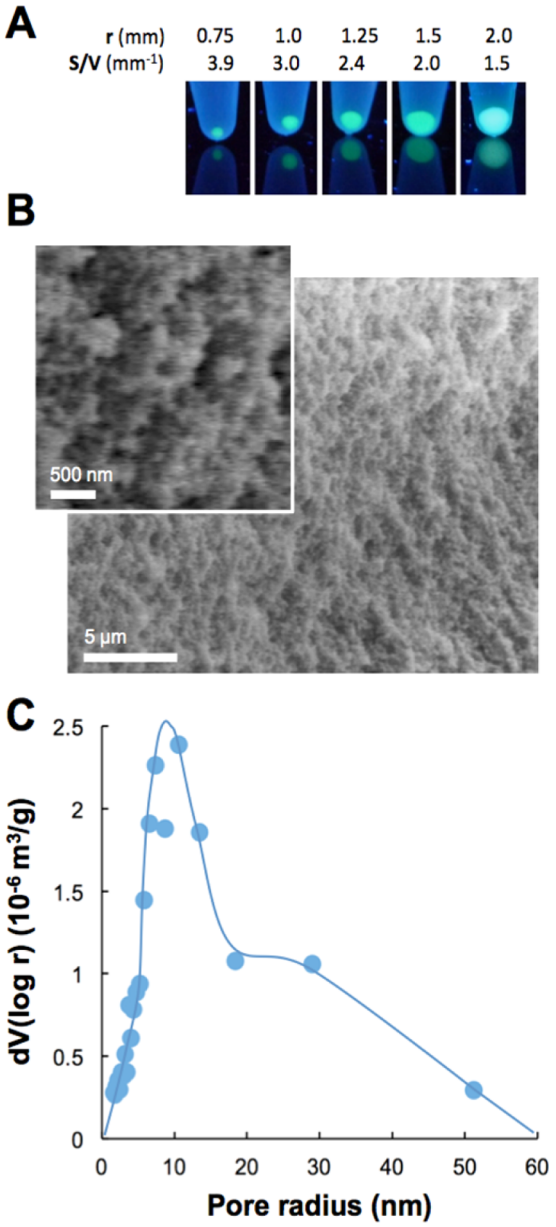

Figure 3. Synthesis and characterization of spherical particles produced in the presence sfGFP-Car9. (A) Appearance of particles of various sizes under UV illumination. (B) SEM images of fractured particles at two magnifications. (C) Pore size distribution of particles subjected to supercritical drying was determined by BJH analysis. The mean pore volume was 1.6 cm^3/g.

region of hemispheroidal particles due to the effect of capillary forces at the air–silica interface.

As expected, arginine supplementation led to efficient release of entrapped sfGFP-Car9 with initial kinetics and extent that increased with decreasing particle size owing to the higher surface to volume ratio (Figures 4 and 3A; Table S2). Under our experimental conditions, ~75% of the protein entrapped in 1 mm radius spheres was released after 24 h incubation with arginine. Half of this amount leached during the first 50 min and only 3% additional release was observed at 48 h. For 2-mm-radius spheres, 65% (respectively, 68%) of the entrapped material was released within 24 h (respectively, 48 h) and half of the loaded protein had reached the supernatant in ~110 min (Figure 4, solid symbols). Fitting of these data with the Ritger-

DOI: 10.1021/acs.bioconjchem.6b00406
Bioconjugate Chem. 2016, 27, 2450–2459

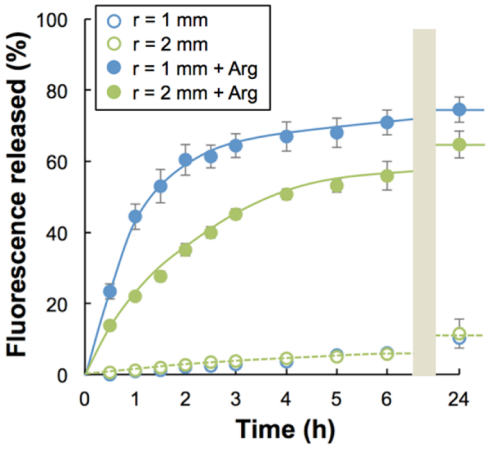

Figure 4. Influence of size on the release of sfGFP-Car9 from spherical sol−gel particles. Protein (10 μM) was entrapped within 1- or 2-mm-radius particles as described in Experimental Procedures. A single 2 mm particle or four 1 mm particles were transferred to 20 mM Tris-HCl, pH 8.5 buffer lacking (open symbols) or containing 1 M arginine (closed symbols). Supernatant fluorescence was assayed at the indicated time points. Error bars correspond to triplicate independent experiments. A value of 100% corresponds to the fluorescence of a 10 μM solution of sfGFP-Car9.

Peppas model[53] (with admittedly unmet assumptions of isotropic medium and perfect sink) provided an estimate for the effective diffusion coefficients ($(1-2) \times 10^{-7}$ cm^2/s; Figure S5). These values are comparable to the diffusivities of horseradish peroxidase ($M_r \sim$ 44-kDa) in silica sol−gels ($(0.5-4) \times 10^{-7}$ cm^2/s)[54] and about 4- to 9-fold lower than the diffusion coefficient of GFP in water (8.7×10^{-7} cm^2/s).[55] Finally, and as expected from the results of Figure 2, the initial kinetics of sfGFP-Car9 release were more than halved when arginine was added to a solution held at pH 7.5 (Table S2, Figure S6).

To obtain additional information on the process of arginine-mediated release, we used confocal fluorescence microscopy to image small and large particles at approximately one-half and one-fourth depth, respectively. Although the entire cross sections were fluorescent at initial time points, some regions were brighter than others, indicating that there is some degree of local variation in sfGFP-Car9 concentration within a confocal slice (Figure 5, top panels). The fusion protein also appeared to be more evenly distributed than in hemispheroidal particles, perhaps because the latter have a less regular pore structure (Figure S3). After 6 h of incubation with arginine, the majority of the remaining fluorescence was confined to the center of the cross-section as would be expected from a typical radial diffusion process. Nevertheless, discrete regions of brightness could be detected (in particular, near the edges of the 2 mm particle at t = 6 h), indicating nonideality in protein release.

Stabilization Effects. Proteins encapsulated in sol−gels typically exhibit enhanced thermodynamic stability relative to their free counterparts due to confinement effects and the and protective microenvironment conferred by the pores.[56,57] In addition, anchoring proteins to surfaces can increase their resistance to unfolding due to a reduction in available conformational degrees of freedom.[58] To determine if our combined entrapment/surface immobilization scheme would increase sfGFP-Car9 thermostability, we exposed particles to temperatures ranging from 70 to 85 °C for 2 h or to increasing

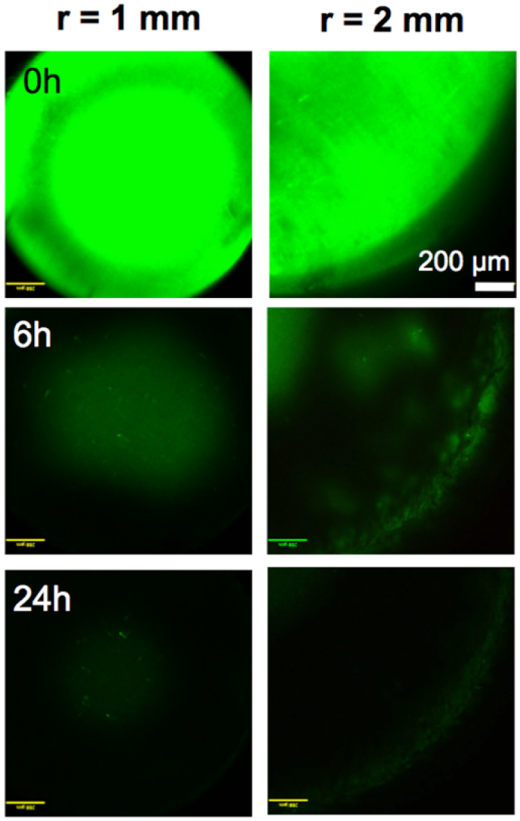

Figure 5. Confocal images of 1- or 2-mm-radius particles loaded with 10 μM sfGFP-Car9 before (0 h) and after 6 and 24 h of incubation in 20 mM Tris-HCl, pH 8.5 supplemented with 1 M arginine. The excitation wavelength was 488 nm. The gains are comparable for all images which leads to overexposure of the 0 h samples. Particle orientation was not maintained.

periods of time at 75 °C. Compared to free sfGFP-Car9, entrapment raised the midpoint unfolding temperature by 4 °C (Figure 6A) and increased the time needed for the protein to experience a 50% decrease in fluorescence at 75 °C from 2 to 5 h (Figure 6B). Although sfGFP denaturation is a fairly complicated two-step process,[59,60] the data of Figure 6 demonstrates that Car9-mediated sequestration within a porous silica network increases sfGFP-Car9 thermostability. It is therefore not surprising that sfGFP-Car9 entrapped in 2 mm spherical sol−gels could be stored at 23 °C in pH 7.5 buffer for at least 6 weeks with less than 10% protein leakage and that the expected 62 ± 5% of original activity could be recovered after 24 h of incubation in pH 8.5 buffer supplemented with arginine.

Release of Multiple Entrapped Proteins. To determine if the Car9 extension would prove useful for the entrapment and controlled release of multiple proteins, sfGFP-Car9 and mCherry-Car9 (a fusion protein between the red fluorescent protein mCherry and the Car9 tag)[43] were mixed at a concentration of 5 μM with prehydrolyzed TMOS and 2-mm-radius spheres were produced by injecting the solution in silicone oil as above. The particles exhibited a uniform yellow−orange color when illuminated at 365 nm, suggesting that the two proteins were homogeneously distributed within the sol−gel matrix (Figure 7A). Consistent with what was observed with sfGFP-Car9 alone (Figure 4), about 12% of the entrapped mCherry-Car9 (and of the coimmobilized sfGFP-Car9) escaped the particles after 24 h of incubation in pH 8.5 buffer (Figure 7B, open symbols). However, at the protein load used

DOI: 10.1021/acs.bioconjchem.6b00406
Bioconjugate Chem. 2016, 27, 2450−2459

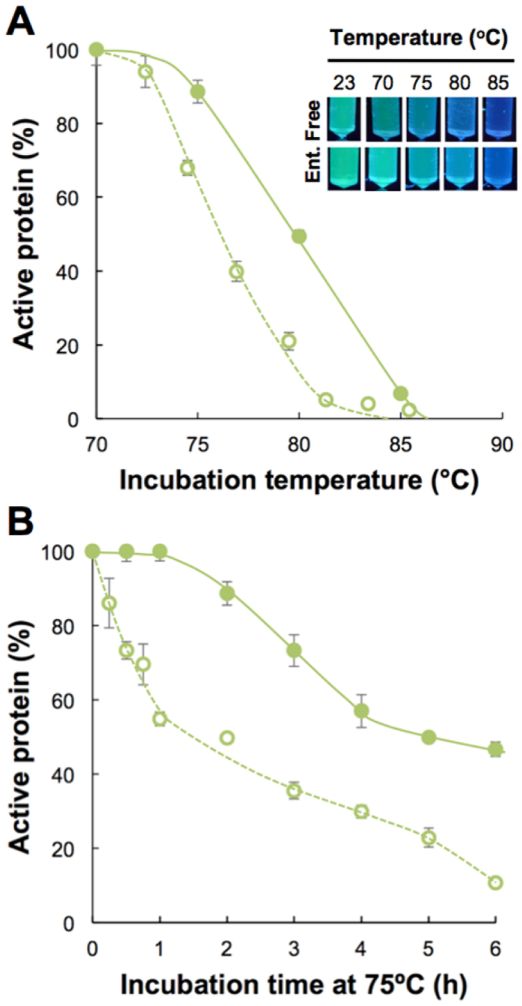

Figure 6. Sol–gel entrapment increases sfGFP-Car9 thermostabiity. (A) Free sfGFP-Car9 (10 μM, open symbols) or 2-mm-radius particles synthesized with 10 μM of the same protein were incubated for 2 h at the indicated temperatures. The entrapped proteins were released by incubation with 1 M arginine for 24 h. The amount of active protein was calculated assuming that 100% activity corresponds to 65% release (see Figure 4). (B) Same as in panel A, except that free protein and particles were incubated at 75 °C for the indicated times.

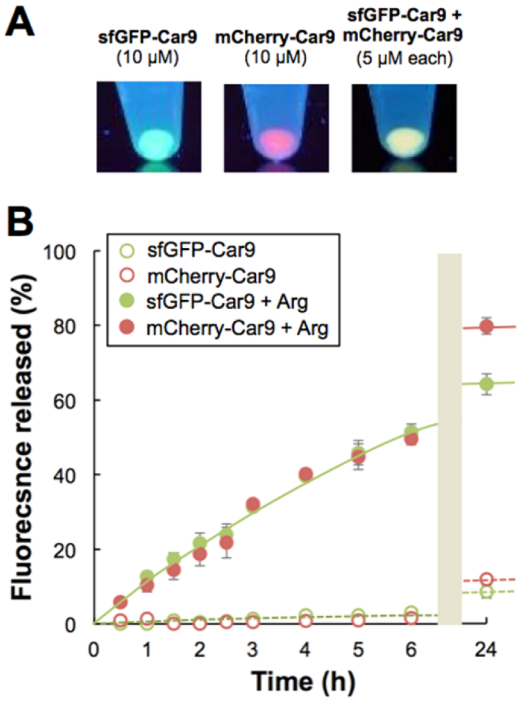

Figure 7. Co-entrapment and release of sfGFP-Car9 and mCherry-Car9. (A) Spherical (r = 2 mm) particles were synthesized in the presence of 10 μM sfGFP-Car9, and 10 μM or 5 μM of each protein. Particles were photographed under UV illumination. (B) A single 2-mm-radius particle was transferred to 20 mM Tris-HCl, pH 8.5 buffer lacking (open symbols) or containing 1 M arginine (closed symbols). The fluorescence in the supernatants was assayed at the indicated time points with excitation at 475 nm (sfGFP-Car9) or 585 nm (mCherry-Car9). Error bars correspond to triplicate independent experiments. A value of 100% corresponds to the fluorescence of a 5 μM solution of sfGFP-Car9 or mCherry-Car9.

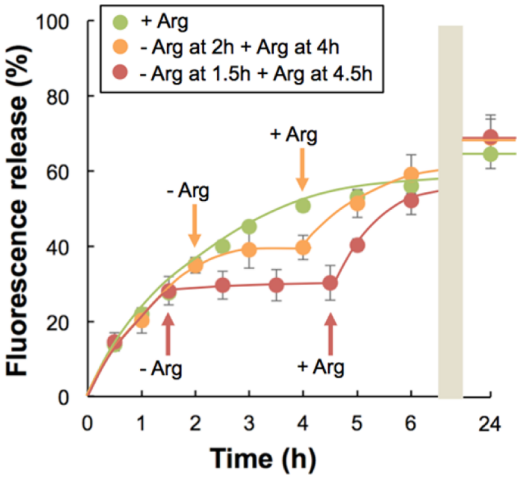

Figure 8. Dynamic control of sfGFP-Car9 release. Spherical (r = 2 mm) particles synthesized in the presence of 10 μM sfGFP-Car9 were incubated in 20 mM Tris-HCl, pH 8.5 supplemented with 1 M arginine for 1.5 or 2 h before being transferred to 20 mM Tris-HCl, pH 8.5 alone. After 2 or 3 h, the particles were once again taken into buffer containing 1 M arginine. The control data set (+ Arg) is identical to that of Figure 4).

in these experiments, little sfGFP-Car9 or mCherry-Car9 made its way into the supernatant in the first 6 h of incubation in buffer. When the particles were exposed to 1 M arginine, both proteins were liberated at nearly identical rates. Protein release was a linear function of time for the first 6 h and initial rates were half those observed when 10 μM sfGFP-Car9 was entrapped in the same particles (compare filled circles in Figures 4 and 7). Taken together, the above results indicate that multiple Car9-tagged proteins can be homogeneously incorporated within silica sol–gels and concomitantly released by arginine treatment. The fact sfGFP-Car9 and mCherry-Car9 are both β-barrel proteins of similar sizes (28.6 vs 30.7 kDa) may explain the similar release kinetics.

Dynamic Control of Protein Release. To determine if sfGFP-Car9 release could be modulated by discontinuous addition of arginine, we prepared 2-mm-radius particles in the presence of 10 μM sfGFP-Car9 and initiated protein release with 1 M arginine as above. However, in these experiments, the buffer was exchanged for Tris-HCl, pH 8.5 after 1.5 or 2 h of incubation. Figure 8 shows that this operation rapidly arrested sfGFP-Car9 release and that there was little evolution of the supernatant fluorescence while the particles were maintained in this buffer. Transfer to arginine solutions after 2 or 3 h restarted

DOI: 10.1021/acs.bioconjchem.6b00406
Bioconjugate Chem. 2016, 27, 2450–2459

the release process with initial kinetics that appeared proportional to the concentration gradient. A similar amount of sfGFP-Car9 was released after 24 h in all cases. This straightforward buffer exchange strategy should be a valuable tool to dynamically control the release of entrapped protein cargos.

CONCLUSION

The Car9 dodecapeptide, which we originally isolated by panning a bacterial cell surface display library against evaporated carbon,[42] has proven a remarkably useful extension: it directs proteins to which it is fused to the edges of graphitic nanostructures,[42] enables their affinity purification on packed silica beds,[43] and allows for on-contact protein patterning on glass substrates.[44] Car9 is considerably shorter than other silica-binding modules that have been used to endow proteins with silica-binding activity,[61−63] which increases its versatility as a fusion tag and simplifies its integration at permissive locations of protein scaffolds to more precisely control protein-inorganic interaction.[38]

In this work, we have exploited the fact that Car9 is less effective at catalyzing silica precipitation than the silaffin-derived R5 peptide to achieve simultaneous surface immobilization and entrapment of Car9-tagged proteins during the formation of silica sol−gels. The resulting matrices have high surface area, support long-term protein storage, and confer enhanced thermostability to cargo polypeptides that are homogeneously distributed within their cores. More uniquely, arginine, which disrupts noncovalent interactions between Car9 extensions and silica surfaces, can be used to turn protein release "on" or "off" with kinetics that are adjustable by manipulating particle geometry, protein load, and solution pH. This simple approach for the production of hybrid silica sol−gel materials that stably encapsulate and release one or more Car9-tagged protein may prove useful for biochemical and medical applications requiring dynamic control of protein concentration.

EXPERIMENTAL PROCEDURES

Protein Purification. *E. coli* BL2(DE3) harboring plasmid pET-24a(+)-sfGFP, pET-24a(+)-sfGFP-Car9, or pET-24a(+)-mCherry-Car9, which encode sfGFP, sfGFP-Car9, or mCherry-Car9 under T7 transcriptional control, respectively,[43] were grown overnight at 37 °C in 25 mL of LB medium supplemented with 50 μg/mL of kanamycin. Seed cultures were used to inoculate 500 mL of supplemented LB, cells were grown at 37 °C to A_{600} ∼ 0.5, and protein expression was induced by addition of 1 mM isopropyl β-D-thiogalactopyranoside (IPTG). Cells were harvested 5 h post-induction by centrifugation at 4000*g* for 10 min. The pellet was resuspended in 35 mL of 20 mM Tris-HCl, pH 7.5 (Buffer A), supplemented with 2 mM EDTA, and disrupted by 6 rounds of sonication for 3 min on a Branson sonifier operated at 30% duty cycle. Lysates were centrifuged at 10 000*g* for 10 min and incubated at 70 °C (sfGFP and sfGFP-Car9) or 50 °C (mCherry-Car9) for 10 min to promote the aggregation of thermolabile host proteins. Insoluble material was removed by centrifugation as above. Car9-tagged proteins were purified by rapid silica-affinity chromatography essentially as described.[43] Briefly, 5 g of silica gel (35−60 mesh, 15 nm pore size, Sigma-Aldrich) equilibrated in Buffer A was packed in a 1-cm-inner-diameter chromatography column (GE Healthcare). Lysates (35 mL) were loaded by aspiration and the column was washed with 30 mL of the same buffer. The protein was eluted with 45 mL of Buffer A supplemented with 1 M arginine. Untagged sfGFP was purified by FPLC on a Whatman DE52 anion exchange cellulose column (GE Healthcare) equilibrated in 20 mM Tris-HCl, pH 8.0 and developed at 1 mL/min. The protein was eluted in 20 mM Tris-HCl, pH 8 supplemented with 1 M NaCl using a 45 mL gradient. Purified proteins were dialyzed against 3L of Buffer A using 10 kDa molecular weight cutoff SnakeSkin tubing (Thermo Scientific) and subjected to 3 buffer changes to ensure complete arginine removal. Proteins were concentrated using 10 kDa microconcentrators (Merck) and stored at −20 °C at a 25 μM final concentration (0.66 mg/mL for sfGFP, 0.71 mg/mL for sfGFP-Car9, and 0.76 mg/mL for mCherry-Car9).

Protein Entrapment in Silica Sol−Gels. A 15 μL aliquot of TMOS (99% purity, 6.6 M; Acros, NJ) was mixed with 40 μL of ddH_2O and 5 μL of 20 mM HCl (20 mM) and the solution was subjected to 5 cycles of 20 s vortexing followed by 40 s rest periods. Proteins (40 μL) were added to the solution at a final concentration of 10 μM (or higher concentration where noted) and a final volume of 100 μL by pipetting.

Hemispheroidal sol−gels particles were produced by depositing 30 μL of the resulting solution on 3.2-mm-diameter polycarbonate filters bounded by a hydrophobic ring and arranged in 96-well format (ChemoTx system, Neuro Probe, Gaithersburg, MD). The filter plates were placed in a chamber sealed with parafilm and sol−gel formation was allowed to proceed for 4 h. The particles were removed with a spatula for long-term storage in 1 mL of Buffer A at room temperature.

Spherical particles were produced by releasing 4.2, 14.1, or 33.5 μL of protein/silicic acid solution from a pipet tip and into 400 μL of silicone oil (poly dimethylsiloxane, CAS:63148−62−9, Pitney Bowes). This led to the formation of particles ∼1, 1.5, or 2 mm in radius, respectively. After 4 h incubation at room temperature, the oil was removed and the particles were washed three times with Buffer A supplemented with 0.02% (w/v) Tween 20 in order to remove residual silicone oil.[52] Samples were stored in 1 mL of Buffer A.

Fluorescence Measurements. To monitor protein release from hemispheroidal sol−gels, samples consisting of a single sfGFP-Car9 or sfGFP particle in 1 mL of Buffer A supplemented or not with 1 M arginine were prepared in triplicate. Tubes were mounted on a Dynabeads rotary sample mixer (Invitrogen) operated at room temperature and 60 rpm. Triplicate samples (100 μL) were harvested at the indicated time points, transferred to a black 96-wells microplate (Greiner), and the fluorescence was measured at 510 nm on a SpectraMax M5 microplate reader (Molecular Devices) with excitation at 475 nm and a cutoff wavelength of 495 nm. All samples were returned to the original tube after measurements with negligible volume loss. Similar experiments were conducted in 20 mM Tris-HCl, pH 8.5 to delineate the influence of pH. Measurements of protein release from spherical sol−gels were performed as above in 20 mM Tris-HCl pH 8.5 except that 4 particles (r = 1 mm), 2 particles (r = 1.5 mm), or a single particle (r = 2 mm) were placed in each tube to allow for easy detection of fluorescence at early time points.

For discontinuous release experiments, a 2-mm-radius silica sol−gel particle loaded with sfGFP-Car9 was placed in 1 mL of 20 mM Tris-HCl, pH 8.5 supplemented with 1 M arginine in triplicate tubes. The fluorescence of the samples was monitored

DOI: 10.1021/acs.bioconjchem.6b00406
Bioconjugate Chem. 2016, 27, 2450−2459

as above except that after 1.5 or 2 h, the supernatant was harvested and reserved. Particles were washed 3 times with 20 mM Tris-HCl, pH 8.5, placed in 1 mL of same buffer and returned to the shaker. The fluorescence of the supernatants and that of the reserved samples were quantified at 1 h intervals. These values were added to produce the plotted data. After 2 or 3 h of incubation in Tris-HCl solutions, beads were retaken in their original arginine-containing buffer and supernatant fluorescence was monitored as above.

For the experiments of Figure 8, sfGFP-Car9 and mCherry-Car9 at 5 μM each were entrapped within 2-mm-radius particles as above. Triplicate tubes containing a single particle were supplemented with 1 mL of 20 mM Tris-HCl, pH 8.5 supplemented, or not with 1 M arginine and protein release was quantified as above for sfGFP-Car9 and using an excitation wavelength of 585 nm, emission wavelength of 625 nm, and a cutoff wavelength of 610 nm for mCherry-Car9. There was negligible bleed-through between fluorescence channels. All samples were photographed under 365 nm excitation using a UV transilluminator.

Thermostability Measurements. Triplicate tubes containing 1 mL of Buffer A and a single 2-mm-radius silica particle loaded with 10 μM sfGFP-Car9 were incubated at 75 °C for the indicated times in a heating block. At the end of each incubation step, particles were transferred to 1 mL of 20 mM Tris-HCl, pH 8.5 supplemented with 1 M arginine, and incubated for 24 h to achieve maximum protein release (~70% of the load). Supernatant fluorescence was measured as above and the fraction of active protein was determined by dividing these numbers by the mean fluorescence released with no heat treatment and 24 h of incubation in 20 mM Tris-HCl, pH 8.5 supplemented with 1 M arginine at room temperature. For control experiments, free sfGFP-Car9 (10 μM in 1 mL of Buffer A) was incubated at 75 °C for the indicated times. The fraction of active protein was determined by dividing the fluorescence at these time points to that of the original solution. Thermostability of entrapped sfGFP-Car9 at high temperatures was determined as above except that the incubation time was set at 2 h.

General Techniques. A Nikon Confocal Microscope A1 and the NIS-Elements AR Microscope Imaging Software were used for acquisition of confocal images with laser excitation at 488 nm. Pore diameters and surface areas were determined on r = 2 mm particles that had been subjected to critical point drying. Briefly, particles were placed in 2 mL of anhydrous ethanol, incubated for 5 days with three solvent exchanges, and loaded on a Quorum E3100 critical point dryer that was filled with CO_2 and held at 10 °C for 2 days. The vessel was periodically purged with ethanol and simultaneously refilled with liquid CO_2. The temperature was raised to 38 °C to ensure that all fluid turned supercritical and the vessel was vented slowly to prevent CO_2 recondensation caused by rapid cooling. After this step, the vessel was allowed to cool naturally to room temperature and the dried particles were heated in vacuum to 160 °C for 12 h to remove adsorbed moisture. A Quantachrome NOVA 2200e pore analyzer wad used to collect the nitrogen isotherm at 77 K. The pore size distribution was obtained by the Barrett−Joyner−Halenda (BJH) method using the instrument software. Surface areas were obtained by the multipoint Brunauer−Emmett−Teller (BET) method, using 6 points in the relative pressure range P/Po = 0.05−0.3. SEM images were acquired on a FEI XL830 dual beam system. Thermogravimetric analysis (TGA) was used to determine the composition of the 2 mm radius spherical particle synthesized in the presence of 10 μM sfGFP-Car9. The sample was dried as previously described, and heated in an aluminum oxide pan from 20 to 850 °C, at a heating rate of 10 °C min^{-1} under the flow of nitrogen gas.

■ ASSOCIATED CONTENT

Supporting Information

The Supporting Information is available free of charge on the ACS Publications website at DOI: 10.1021/acs.bioconjchem.6b00406.

Supplementary Figures S1 to S6 and Tables S1 and S2 (PDF)

■ AUTHOR INFORMATION

Corresponding Author

*E-mail: baneyx@uw.edu.

Notes

The authors declare the following competing financial interest(s): The technology described herein is being patented.

■ ACKNOWLEDGMENTS

This work was supported by the Charles W. H. Matthaei endowment and in part by the Office of Naval Research award BRC-11123566 and NSF award BBBE 1401835. We are indebted to Matthew Lim and Peter Pauzauskie for their help with BET measurements and to Brian Swift for collecting the data of Figure S1. Part of this work was conducted at the University of Washington Molecular Analysis Facility, a member of the NSF-supported National Nanotechnology Infrastructure Network.

■ REFERENCES

(1) Manzano, M., and Vallet-Regi, M. (2010) New developments in ordered mesoporous materials for drug delivery. *J. Mater. Chem. 20*, 5593−5604.

(2) Buthe, A. (2011) Entrapment of enzymes in nanoporous sol-gels. *Methods Mol. Biol. 743*, 223−37.

(3) Wang, X., Ahmed, N. B., Alvarez, G. S., Tuttolomondo, M. V., Helary, C., Desimone, M. F., and Coradin, T. (2015) Sol-gel encapsulation of biomolecules and cells for medicinal applications. *Curr. Top. Med. Chem. 15*, 223−44.

(4) Wang, Y., Zhao, Q., Han, N., Bai, L., Li, J., Liu, J., Che, E., Hu, L., Zhang, Q., Jiang, T., and Wang, S. (2015) Mesoporous silica nanoparticles in drug delivery and biomedical applications. *Nanomedicine 11*, 313−27.

(5) Brinker, C. J., and Scherer, G. W. (1990) *Sol-Gel Science. The Physics and Chemistry of Sol-Gel Processing*, Academic Press, San Diego.

(6) Belton, D. J., Deschaume, O., and Perry, C. C. (2012) An overview of the fundamentals of the chemistry of silica with relevance to biosilicification and technological advances. *FEBS J. 279*, 1710−20.

(7) Ciriminna, R., Fidalgo, A., Pandarus, V., Beland, F., Ilharco, L. M., and Pagliaro, M. (2013) The sol-gel route to advanced silica-based materials and recent applications. *Chem. Rev. 113*, 6592−620.

(8) Avnir, D., Braun, S., Lev, O., and Ottolenghi, M. (1994) Enzymes and Other Proteins Entrapped in Sol-Gel Materials. *Chem. Mater. 6*, 1605−1614.

(9) Bhatia, R. B., Brinker, C. J., Gupta, A. K., and Singh, A. K. (2000) Aqueous sol-gel process for protein encapsulation. *Chem. Mater. 12*, 2434−2441.

(10) Coradin, T., and Lopez, P. J. (2003) Biogenic silica patterning: simple chemistry or subtle biology? *ChemBioChem 4*, 251−9.

(11) Kandimalla, V. B., Tripathi, V. S., and Ju, H. X. (2006) Immobilization of biomolecules in sol-gels: Biological and analytical applications. *Crit. Rev. Anal. Chem. 36*, 73−106.

DOI: 10.1021/acs.bioconjchem.6b00406
Bioconjugate Chem. 2016, 27, 2450−2459

(12) Wu, S. H., Mou, C. Y., and Lin, H. P. (2013) Synthesis of mesoporous silica nanoparticles. *Chem. Soc. Rev. 42*, 3862−3875.
(13) Huang, Z. H., and Che, S. N. (2015) Fabrication of Mesostructured Silica Materials through Co-Structure-Directing Route. *Bull. Chem. Soc. Jpn. 88*, 617−632.
(14) Malgras, V., Ji, Q. M., Kamachi, Y., Mori, T., Shieh, F. K., Wu, K. C. W., Ariga, K., and Yamauchi, Y. (2015) Templated Synthesis for Nanoarchitectured Porous Materials. *Bull. Chem. Soc. Jpn. 88*, 1171−1200.
(15) Song, N., and Yang, Y. W. (2015) Molecular and supramolecular switches on mesoporous silica nanoparticles. *Chem. Soc. Rev. 44*, 3474−3504.
(16) Sun, L. B., Liu, X. Q., and Zhou, H. C. (2015) Design and fabrication of mesoporous heterogeneous basic catalysts. *Chem. Soc. Rev. 44*, 5092−5147.
(17) Slowing, I. I., Trewyn, B. G., Giri, S., and Lin, V. S. Y. (2007) Mesoporous silica nanoparticles for drug delivery and biosensing applications. *Adv. Funct. Mater. 17*, 1225−1236.
(18) Pierre, A. C. (2004) The sol-gel encapsulation of enzymes. *Biocatal. Biotransform. 22*, 145−170.
(19) Mamaeva, V., Sahlgren, C., and Linden, M. (2013) Mesoporous silica nanoparticles in medicine−recent advances. *Adv. Drug Delivery Rev. 65*, 689−702.
(20) Kroger, N., and Poulsen, N. (2008) Diatoms-from cell wall biogenesis to nanotechnology. *Annu. Rev. Genet. 42*, 83−107.
(21) Sahebi, M., Hanafi, M. M., Siti Nor Akmar, A., Rafii, M. Y., Azizi, P., Tengoua, F. F., Nurul Mayzaitul Azwa, J., and Shabanimofrad, M. (2015) Importance of silicon and mechanisms of biosilica formation in plants. *BioMed Res. Int. 2015*, 396010.
(22) Kroger, N., Deutzmann, R., and Sumper, M. (1999) Polycationic peptides from diatom biosilica that direct silica nanosphere formation. *Science 286*, 1129−1132.
(23) Lechner, C. C., and Becker, C. F. (2015) Silaffins in Silica Biomineralization and Biomimetic Silica Precipitation. *Mar. Drugs 13*, 5297−333.
(24) Naik, R. R., Whitlock, P. W., Rodriguez, F., Brott, L. L., Glawe, D. D., Clarson, S. J., and Stone, M. O. (2003) Controlled formation of biosilica structures in vitro. *Chem. Commun. (Cambridge, U. K.)*, 238−9.
(25) Ravera, E., Martelli, T., Geiger, Y., Fragai, M., Goobes, G., and Luchinat, C. (2016) Biosilica and bioinspired silica studied by solid-state NMR. *Coord. Chem. Rev.*, DOI: 10.1016/j.ccr.2016.06.003.
(26) Knecht, M. R., and Wright, D. W. (2003) Functional analysis of the biomimetic silica precipitating activity of the R5 peptide from Cylindrotheca fusiformis. *Chem. Commun. (Cambridge, U. K.)*, 3038−9.
(27) Lechner, C. C., and Becker, C. F. (2014) A sequence-function analysis of the silica precipitating silaffin R5 peptide. *J. Pept. Sci. 20*, 152−8.
(28) Luckarift, H. R., Spain, J. C., Naik, R. R., and Stone, M. O. (2004) Enzyme immobilization in a biomimetic silica support. *Nat. Biotechnol. 22*, 211−3.
(29) Naik, R. R., Tomczak, M. M., Luckarift, H. R., Spain, J. C., and Stone, M. O. (2004) Entrapment of enzymes and nanoparticles using biomimetically synthesized silica. *Chem. Commun. (Cambridge, U. K.)*, 1684−5.
(30) Lechner, C. C., and Becker, C. F. (2013) Modified silaffin R5 peptides enable encapsulation and release of cargo molecules from biomimetic silica particles. *Bioorg. Med. Chem. 21*, 3533−41.
(31) Choi, O., Kim, B. C., An, J. H., Min, K., Kim, Y. H., Um, Y., Oh, M. K., and Sang, B. I. (2011) A biosensor based on the self-entrapment of glucose oxidase within biomimetic silica nanoparticles induced by a fusion enzyme. *Enzyme Microb. Technol. 49*, 441−5.
(32) Marner, W. D., 2nd, Shaikh, A. S., Muller, S. J., and Keasling, J. D. (2009) Enzyme immobilization via silaffin-mediated autoencapsulation in a biosilica support. *Biotechnol. Prog. 25*, 417−23.
(33) Nam, D. H., Won, K., Kim, Y. H., and Sang, B. I. (2009) A novel route for immobilization of proteins to silica particles incorporating silaffin domains. *Biotechnol. Prog. 25*, 1643−9.
(34) Luckarift, H. R., Dickerson, M. B., Sandhage, K. H., and Spain, J. C. (2006) Rapid, room-temperature synthesis of antibacterial bionanocomposites of lysozyme with amorphous silica or titania. *Small 2*, 640−3.
(35) Baneyx, F., and Schwartz, D. T. (2007) Selection and analysis of solid-binding peptides. *Curr. Opin. Biotechnol. 18*, 312−317.
(36) Care, A., Bergquist, P. L., and Sunna, A. (2015) Solid-binding peptides: smart tools for nanobiotechnology. *Trends Biotechnol. 33*, 259−68.
(37) Chen, C. L., and Rosi, N. L. (2010) Peptide-Based Methods for the Preparation of Nanostructured Inorganic Materials. *Angew. Chem., Int. Ed. 49*, 1924−1942.
(38) Coyle, B. L., Zhou, W., and Baneyx, F. (2013) Protein-aided mineralization of inorganic nanostructures, in *Bionanotechnology: biological self-assembly and its applications* (Rehm, B. H. A., Ed.) Caister Academic Press, Norwich, U.K.
(39) Dickerson, M. B., Sandhage, K. H., and Naik, R. R. (2008) Protein- and peptide directed synthesis of inorganic materials. *Chem. Rev. 108*, 4935−4978.
(40) Sarikaya, M., Tamerler, C., Jen, A. K., Schulten, K., and Baneyx, F. (2003) Molecular biomimetics: nanotechnology through biology. *Nat. Mater. 2*, 577−585.
(41) Tamerler, C., Khatayevich, D., Gungormus, M., Kacar, T., Oren, E. E., Hnilova, M., and Sarikaya, M. (2010) Molecular biomimetics: GEPI-based biological routes to technology. *Biopolymers 94*, 78−94.
(42) Coyle, B. L., Rolandi, M., and Baneyx, F. (2013) Carbon-binding designer proteins that discriminate between sp2- and sp3-hybridized carbon surfaces. *Langmuir 29*, 4839−4846.
(43) Coyle, B. L., and Baneyx, F. (2014) A cleavable silica-binding affinity tag for rapid and inexpensive protein purification. *Biotechnol. Bioeng. 111*, 2019−26.
(44) Coyle, B. L., and Baneyx, F. (2016) Direct and reversible immobilization and microcontact printing of functional proteins on glass using a genetically appended silica-binding tag. *Chem. Commun. (Cambridge, U. K.) 52*, 7001−4.
(45) Pedelacq, J. D., Cabantous, S., Tran, T., Terwilliger, T. C., and Waldo, G. S. (2006) Engineering and characterization of a superfolder green fluorescent protein. *Nat. Biotechnol. 24*, 79−88.
(46) Wieneke, R., Bernecker, A., Riedel, R., Sumper, M., Steinem, C., and Geyer, A. (2011) Silica precipitation with synthetic silaffin peptides. *Org. Biomol. Chem. 9*, 5482−5486.
(47) Zhou, W., Schwartz, D. T., and Baneyx, F. (2010) Single pot biofabrication of zinc sulfide immuno-quantum dots. *J. Am. Chem. Soc. 132*, 4731−4738.
(48) Emami, F. S., Puddu, V., Berry, R. J., Varshney, V., Patwardhan, S. V., Perry, C. C., and Heinz, H. (2014) Force Field and a Surface Model Database for Silica to Simulate Interfacial Properties in Atomic Resolution. *Chem. Mater. 26*, 2647−2658.
(49) Davis, P. J., Brinker, C. J., and Smith, D. M. (1992) Pore Structure Evolution in Silica-Gel during Aging Drying. I. Temporal and Thermal Aging. *J. Non-Cryst. Solids 142*, 189−196.
(50) Davis, P. J., Brinker, C. J., Smith, D. M., and Assink, R. A. (1992) Pore Structure Evolution in Silica-Gel during Aging Drying. II. Effect of Pore Fluids. *J. Non-Cryst. Solids 142*, 197−207.
(51) Santos, E. M., Radin, S., and Ducheyne, P. (1999) Sol-gel derived carrier for the controlled release of proteins. *Biomaterials 20*, 1695−700.
(52) Dixit, N., Maloney, K. M., and Kalonia, D. S. (2012) The effect of Tween((R)) 20 on silicone oil-fusion protein interactions. *Int. J. Pharm. 429*, 158−67.
(53) Ritger, P. L., and Peppas, N. A. (1987) A simple equation for description of solute release I. Fickian and non-Fickian release from non-swellable devices in the form of slabs, spheres, cylinders or discs. *J. Controlled Release 5*, 23−36.
(54) Hungerford, G., Rei, A., Ferreira, M. I., Suhling, K., and Tregidgo, C. (2007) Diffusion in a sol-gel-derived medium with a view toward biosensor applications. *J. Phys. Chem. B 111*, 3558−62.

DOI: 10.1021/acs.bioconjchem.6b00406
Bioconjugate Chem. 2016, 27, 2450−2459

(55) Dayel, M. J., Hom, E. F., and Verkman, A. S. (1999) Diffusion of green fluorescent protein in the aqueous-phase lumen of endoplasmic reticulum. *Biophys. J. 76*, 2843−51.
(56) Zheng, L., and Brennan, J. D. (1998) Measurement of intrinsic fluorescence to probe the conformational flexibility and thermodynamic stability of a single tryptophan protein entrapped in a sol-gel derived glass matrix. *Analyst 123*, 1735−1744.
(57) Zheng, L. L., Reid, W. R., and Brennan, J. D. (1997) Measurement of fluorescence from tryptophan to probe the environment and reaction kinetics within protein-doped sol-gel-derived glass monoliths. *Anal. Chem. 69*, 3940−3949.
(58) Singh, R. K., Tiwari, M. K., Singh, R., and Lee, J. K. (2013) From protein engineering to immobilization: promising strategies for the upgrade of industrial enzymes. *Int. J. Mol. Sci. 14*, 1232−77.
(59) Campanini, B., Bologna, S., Cannone, F., Chirico, G., Mozzarelli, A., and Bettati, S. (2005) Unfolding of Green Fluorescent Protein mut2 in wet nanoporous silica gels. *Protein Sci. 14*, 1125−33.
(60) Hsu, S. T., Blaser, G., and Jackson, S. E. (2009) The folding, stability and conformational dynamics of beta-barrel fluorescent proteins. *Chem. Soc. Rev. 38*, 2951−65.
(61) Bolivar, J. M., and Nidetzky, B. (2012) Positively charged mini-protein Zbasic2 as a highly efficient silica binding module: opportunities for enzyme immobilization on unmodified silica supports. *Langmuir 28*, 10040−9.
(62) Sunna, A., Chi, F., and Bergquist, P. L. (2013) A linker peptide with high affinity towards silica-containing materials. *New Biotechnol. 30*, 485−92.
(63) Taniguchi, K., Nomura, K., Hata, Y., Nishimura, T., Asami, Y., and Kuroda, A. (2007) The Si-tag for immobilizing proteins on a silica surface. *Biotechnol. Bioeng. 96*, 1023−9.

DOI: 10.1021/acs.bioconjchem.6b00406
Bioconjugate Chem. 2016, 27, 2450−2459